Wide-Area backup protection against asymmetrical faults in the presence of renewable energy sources

Mohammad Rezaei Jegarluei [a,*], Petros Aristidou [b], Sadegh Azizi [a]

[a] *School of Electronic and Electrical Engineering, University of Leeds, Leeds LS2 9JT, UK*
[b] *Department of Electrical Engineering, Computer Engineering and Informatics, Cyprus University of Technology, Limassol 3036, Cyprus*

ARTICLE INFO

ABSTRACT

Conventional protection schemes have essentially been developed for power systems dominated by synchronous generators. High penetration of power-electronic interfaced renewable energy sources (PEIRESs) can adversely impact the reliability of protection systems, thereby increasing the risk of widespread disturbances. This paper proposes a robust wide-area backup protection (WABP) scheme against asymmetrical faults for transmission systems with high penetration of renewables. The scheme exploits the full potential of available synchrophasors without placing any rigid constraints on PMU locations. To this end, the faulted line and a few appropriately selected PEIRESs are replaced by equivalent current sources using the Substitution Theorem. The remaining PEIRESs are substituted by their equivalent impedances accounting for their response to a fault, considering the control strategies and overcurrent limits of these PEIRESs. This results in a linear system of equations whose solution readily indicates the faulted line on account of the weighted sum of squared residuals (*WSSR*) concept. To add to the security of the proposed scheme, the fault distance on the pinpointed line is also calculated and checked to ensure it lies within the acceptable range. A total of more than 80,000 simulations conducted on the IEEE 39-bus test system verify that the proposed scheme performs properly irrespective of the numbers/locations of PEIRESs and their control strategies.

1. Introduction

The reliability of protection schemes is of utmost importance to the secure operation of power systems in the face of different contingencies. Dependability and security are key aspects characterizing the reliability of a well-designed protection scheme [1]. Local protection schemes are not ideal and their reliability may occasionally be compromised for different reasons. At the forefront of these are measurement errors caused by transient behavior of voltage and current transformers located close to the fault location [2]. Some research works are aimed at complementing the efficacy of local protection by leveraging synchrophasors provided by Phasor Measurement Units (PMUs). In this context, Wide-Area Backup Protection (WABP) is defined as the processing of phasors provided by PMUs and other intelligent electronic devices to identify the faulted line and generate appropriate protection commands accounting for local protection failures.

Operation philosophies of conventional protection schemes have mainly been developed for power systems dominated by conventional synchronous machines. On the other hand, Power Electronic Interfaced

Renewable Energy Sources (PEIRESs) demonstrate exclusive fault characteristics that significantly differ from those of synchronous generators. Thus, high penetration of renewables is making some underlying assumptions of conventional protection schemes increasingly invalid. This can adversely affect the performance of protection systems, which is demonstrated by more cases of maloperation/malfunction of protective relays [3–5]. For instance, the distinctive negative-sequence fault current contribution of renewables can easily mislead the negative-sequence overcurrent and communication-assisted protections following asymmetrical faults [6,7]. Improving the reliability of protection schemes in the presence of renewable energy sources has received remarkable attention in recent years [8–11]. To overcome the protection challenges introduced by renewables, more sophisticated local/wide-area schemes with adaptive features are needed.

Due to the inherent limitations of WABP, e.g., originated from communication latencies, WABP is not supposed to replace the local main/backup protection but complement it [12]. WABP has a great potential to add an extra layer of defense against faults, thereby enhancing system stability. WABP schemes in [13–15] need PMU data
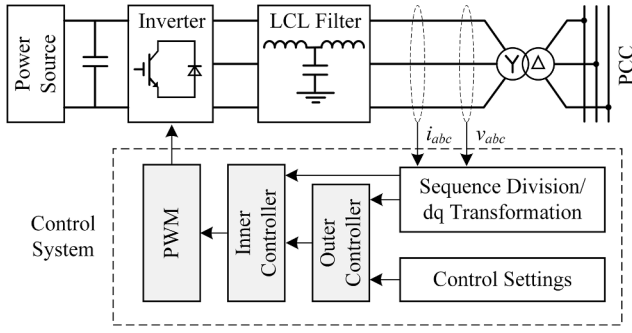

Fig. 1. PEIRES configuration and power control scheme.

from certain locations and cannot tolerate PMU losses. The schemes in [16–21] are based on the superimposed circuit methodology [22]. None of these schemes account for renewable energy sources assuming all generating units are synchronous machines. In these schemes, synchronous machines are usually modeled by a constant impedance in the superimposed circuit. However, this does not apply to PEIRESs because of their time-variant nature and distinguished fault behavior. To utilize the schemes in [13–23], one needs to disregard the presence of PEIRESs in the power system. However, simulations show that this approach might easily lead to misoperation or malfunction of the WABP scheme.

PEIRESs are characterized by their controllability features, which are not accounted for by the existing superimposed-circuit-based WAPB schemes. PEIRESs can rapidly regulate the amplitude and phase angle of their terminal voltage and current to meet their control targets in the steady-state, fault, and post-fault conditions within a few milliseconds [24]. There are some efforts in the literature to incorporate PEIRESs in WABP schemes. A communication-free active protection strategy for the inverter-dominated power systems is presented in [25], which is only applicable for islanded microgrids. In [26], a WABP scheme is presented as a supervisory algorithm for distance relay, which requires a specific set of PMU measurements. A reliable WABP scheme should be able to capture the behavior of PEIRESs while maintaining the computational burden low. This paper addresses these challenges without placing any constraint on the number and locations of PEIRESs or their control strategies.

In this paper, a novel WABP scheme is proposed against asymmetrical faults on transmission systems with high penetration of PEIRESs. The proposed scheme leverages the full potential of available synchrophasors without placing any strict constraints on PMU locations. The scheme performs well under a wide variety of control strategies employed by PEIRESs. To enable this, PEIRESs are appropriately modeled to capture their fault behavior, thus formulating their impact on the WABP.

The remainder of this paper is organized as follows. Section II describes the PEIRES configuration and related power control strategies. Section III puts forward the proposed scheme for WABP. Modifications applied to overcome large numbers of PEIRESs are detailed in Section IV. Extensive simulation studies are conducted and discussed in Section V. Finally, the paper is concluded in Section VI.

2. PEIRES configuration and power control strategy

This section presents the PEIRES configuration studied and the power control strategies scrutinized in the following sections. It is assumed that a standard three-phase Voltage Source Converter (VSC) is connected to the Point of Common Coupling (PCC) and the grid through an LCL filter, as shown in Fig. 1. Such PEIRESs are typically controlled by a three-level control structure, including the outer control loops, inner current control loop, and the PWM controller [24]. The outer control loops determine current references for the inner current control loop, which translates these to voltage references for the PWM

controller.

Without loss of generality, in this paper, the dual reference frame scheme presented in [27] is used for the outer control loops of PEIRESs. In this approach, the positive rotating synchronous frame is utilized to control the positive-sequence components. The negative rotating synchronous frame is also used to control the negative-sequence components. In doing so, the converter voltages and currents in the stationary *abc* frame are first expressed in terms of the stationary $\alpha\beta$ reference frame [24,27]. Then, the positive- and negative-sequence quantities in the $\alpha\beta$ frame are obtained. For example, voltage quantities are calculated as shown below.

$$\begin{bmatrix} v_\alpha{}^p \\ v_\beta{}^p \end{bmatrix} = \frac{1}{2}\begin{bmatrix} 1 & -i \\ i & 1 \end{bmatrix}\begin{bmatrix} v_\alpha \\ v_\beta \end{bmatrix}$$

$$\begin{bmatrix} v_\alpha{}^n \\ v_\beta{}^n \end{bmatrix} = \frac{1}{2}\begin{bmatrix} 1 & i \\ -i & 1 \end{bmatrix}\begin{bmatrix} v_\alpha \\ v_\beta \end{bmatrix} \tag{1}$$

where the operator i represents a $90°$ phase shift in the time domain, and the superscripts p and n refer to positive- and negative- sequence components, respectively. Finally, the $\alpha\beta$ stationary frame quantities are transformed into their respective sequence rotating dq-frames, i.e. $v_d{}^p$, $v_q{}^p$, $v_d{}^n$, and $v_q{}^n$ [24].

Within the three-level control structure, the outer control loops have the duty of adjusting the average active and reactive power of the PEIRES in normal operating conditions [24]. However, some extra control loops can be appended to the outer control loop to appropriately respond to fault conditions in the positive- and negative-sequence circuits. While the Grid Code typically dictates positive-sequence control references, negative-sequence quantities may be controlled as appropriate with no strict requirements in place. Popular control objectives for the negative-sequence circuit are suppressing the negative-sequence current, eliminating the active power ripple, eliminating the reactive power ripple, or imitating an impedance in the negative-sequence circuit [28,29]. These control strategies aimed at unbalanced voltage conditions are detailed below.

A. Suppressing Negative-Sequence Current

If the negative-sequence voltage at the VSC terminal is not controlled, it remains zero in all operating conditions. This can result in a large damaging negative-sequence current passing through the VSC upon an asymmetrical fault. A reasonable preventative strategy is to eliminate the negative-sequence current passing through the VSC. To this end, the negative-sequence references are set to zero, while the positive-sequence current references are regulated by the Grid Code. A key feature of this strategy is the retention of the maximum current capacity of the PEIRES for control purposes in the positive-sequence circuit [28].

B. Eliminating the Active or Reactive Power Ripple

The power ripple refers to the oscillating components of active or reactive power during faults. It is possible to remove the power ripple using appropriate negative-sequence control strategies. To this end, the reference currents are calculated as below [28]:

$$\begin{bmatrix} i_d{}^p \\ i_q{}^p \\ i_d{}^n \\ i_q{}^n \end{bmatrix}_{ref} = \begin{bmatrix} v_d{}^p & v_q{}^p \\ v_q{}^p & -v_d{}^p \\ -Kv_d{}^n & Kv_q{}^n \\ -Kv_q{}^n & -Kv_d{}^n \end{bmatrix}\begin{bmatrix} \dfrac{P_{ref}}{D} \\ \dfrac{Q_{ref}}{E} \end{bmatrix} \tag{2}$$

where P_{ref} and Q_{ref} are the reference values for the active and reactive

power, and the coefficients D and E are calculated based on the PEIRES control strategy and quantities in the rotating dq-frames as below.

$$\begin{cases} D = (v_d{}^p)^2 + \left(v_q{}^p\right)^2 - K(v_d{}^n)^2 - K\left(v_q{}^n\right)^2 \\ E = (v_d{}^p)^2 + \left(v_q{}^p\right)^2 + K(v_d{}^n)^2 + K\left(v_q{}^n\right)^2 \end{cases} \tag{3}$$

The coefficient K in the forgoing formulas is set to -1 when the control strategy is eliminating the active power ripple. This coefficient is set to 1 when the control strategy is eliminating the reactive power ripple.

C. Imitating an Impedance in the Negative-Sequence Circuit

The most recent German Grid Code [30] requires the negative-sequence current to be injected in proportion to the negative-sequence voltage. This would help directional protection elements operate reliably by providing sufficient negative-sequence current and a noticeable phase angle difference between negative-sequence voltage and current [7]. If the negative-sequence current is maintained proportional to negative-sequence voltage, the PEIRES demonstrates a constant negative-sequence impedance, i.e. $|z^n| \angle \theta^n$. To achieve this, the reference currents are obtained from.

$$\begin{bmatrix} i_d{}^n \\ i_q{}^n \end{bmatrix}_{ref} = \begin{bmatrix} v_d{}^n & v_q{}^n \\ v_q{}^n & -v_d{}^n \end{bmatrix} \begin{bmatrix} \dfrac{cos(\theta^n)}{|z^n|} \\ \dfrac{sin(\theta^n)}{|z^n|} \end{bmatrix} \tag{4}$$

3. **The proposed superimposed circuit technique**

In this section, the superimposed circuit technique presented in [18] is extended to derive a linear system of equations for WABP concerning the fault incident. Phasor measurements and the bus impedance matrix are the inputs to the scheme. A prerequisite for using the superimposed circuit is that the pre-disturbance and post-disturbance bus impedance matrices remain the same, which is not the case when the disturbance is a short-circuit fault on a line. To overcome this challenge, the candidate faulted line is replaced by two current sources prior to and following the fault inception [18]. Therefore, the faulted line and fault resistance are not included in the bus impedance matrix, while their effects are reflected in the current sources. Synchronous generators can be modeled as constant impedances in the superimposed circuit within the time frame of interest [15,17]. However, this is not valid for renewables due to their time-variant nature induced by their control strategies. Therefore, PEIRESs are replaced by proper current sources in this study. As a result, the superimposed circuit will include two nodal current injections representing the faulted line and a nodal current injection for each PEIRES to represent its behavior with reference to the fault. Then, the Weighted Sum of Squared Residuals (*WSSR*) is used to pinpoint the faulted line, as explained in Subsection III-C.

A. Individual Analysis of the Sequence Circuits

The interconnection of sequence circuits is dictated by the fault type [2]. Nonetheless, each sequence circuit can also be studied independently regardless of the fault resistance, type, and location. This is possible so long as the other sequence circuits and fault resistance are replaced by a proper current source based on the Substitution Theorem [18].

Asymmetrical faults are the most frequent type of short-circuit faults on transmission systems [2]. The focus of this paper is WABP against asymmetrical faults by taking advantage of the unique characteristics of the negative-sequence circuit [19]. The negative-sequence circuit is the most suitable circuit for fault location analysis under asymmetrical
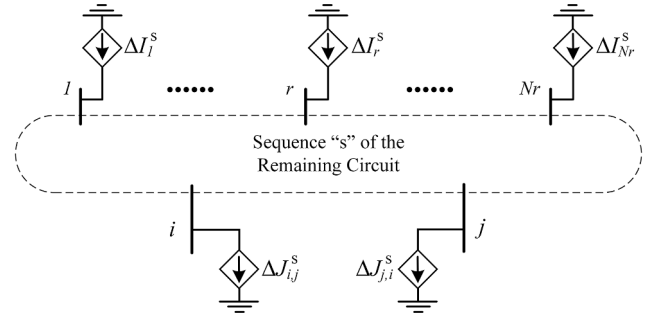

Fig. 2. Superimposed sequence circuit for a fault at line i-j.

faults. This is due to the absence of negative-sequence components in the pre-fault condition, the time-invariant behavior of synchronous machines in the negative-sequence circuit, and its higher accuracy compared to that of the zero-sequence circuit [19]. As will be described in Section IV, the positive-sequence circuit will only be employed for identifying the operating modes of PEIRESs.

B. Systems of Equations Representing the Fault

As shown in Fig. 2, let us assume that line i-j is the faulted line and Z^s denotes the bus impedance matrix of the sequence circuit "s" excluding line i-j and all PEIRESs. The superscript s refers to the corresponding sequence circuit and takes a value of "p" or "n" for the positive- and negative-sequence circuits, respectively. Let ΔI_r^s, $\Delta J_{i,j}^s$, and $\Delta J_{j,i}^s$ represent the superimposed current of a PEIRES at bus r and those of the sending- and receiving-end of the faulted line i-j, respectively. The superimposed voltage measured by a PMU at an arbitrary bus k satisfies the following equation.

$$\Delta V_k^{s,m} = \sum_{r=1}^{Nr} Z_{k,r}^s \Delta I_r^s - Z_{k,i}^s \Delta J_{i,j}^s - Z_{k,j}^s \Delta J_{j,i}^s + e_{V(k)} \tag{5}$$

where the superscript "m" refers to measured quantities, 1 to Nr are the indices of buses connected to a PEIRES, and $e_{V(k)}$ represents the associated measurement error.

Let $\Delta J_{u,v}^s$ denote the PMU-measured superimposed current of the sending-end of a non-faulted line u-v. This current can be expressed as a function of the nodal current sources as below.

$$\Delta J_{uv}^{s,m} = \sum_{r=1}^{Nr} C_{uv,r}^s \Delta I_r^s - C_{uv,i}^s \Delta J_{i,j}^s - C_{uv,j}^s \Delta J_{j,i}^s + e_{J(uv)} \tag{6}$$

where $e_{J(uv)}$ stands for the corresponding measurement error, and the derivation of C_{uv}^s is detailed in [18]. Subject to the direct measurement of ΔI_r^s, $\Delta J_{i,j}^s$, and $\Delta J_{j,i}^s$ by PMUs, the equations below can also be established.

$$\begin{cases} \Delta I_r^{s,m} = \Delta I_r^s + e_{I(r)} \\ \Delta J_{i,j}^{s,m} = -\Delta J_{i,j}^s + e_{J(ij)} \\ \Delta J_{j,i}^{s,m} = -\Delta J_{j,i}^s + e_{J(ji)} \end{cases} \tag{7}$$

where the negative signs on the right-hand side of the equations result from the convention assumed for the direction of nodal injections and transmission line currents. It should be noted that Fig. 2 is only an exemplary representation of the superimposed circuit. Equations (5) to (7) remain valid even when either or both of buses i and j is connected to a PEIRES.

Let us assume PMUs provide Np voltage and current measurements from across the grid. By writing equations (5) to (7) based on available PMU measurements, a system of linear equations can be obtained as below.

$$\boldsymbol{m}_{Np\times 1} = \boldsymbol{H}_{Np\times(2+Nr)}\boldsymbol{x}_{(2+Nr)\times 1} + \boldsymbol{\varepsilon}_{Np\times 1} \tag{8}$$

where $\boldsymbol{m}$, $\boldsymbol{H}$, and $\boldsymbol{\varepsilon}$ are the measurement vector, coefficient matrix, and error vector, respectively. Further, $\boldsymbol{x}$ is the vector of current sources replaced for the faulted line and PEIRESs, as below.

$$\boldsymbol{x} = \begin{bmatrix} \Delta J_{i,j}^s & \Delta J_{i,j}^s & \Delta I_1^s & \cdots & \Delta I_{Nr}^s \end{bmatrix}^T \tag{9}$$

Let $\boldsymbol{R}$ denote the covariance matrix of measurement errors, which is an Np-by-Np diagonal matrix whose i-th diagonal entry is the variance of the i-th measurement. The linear system of equations (8) can be readily solved using the weighted least-squares method as follows.

$$\hat{\boldsymbol{x}} = \left(\boldsymbol{H}^*\boldsymbol{R}^{-1}\boldsymbol{H}\right)^{-1}\boldsymbol{H}^*\boldsymbol{R}^{-1}\boldsymbol{m} \tag{10}$$

where the asterisk on $\boldsymbol{H}$ refers to the conjugate transpose of that matrix. The vector $\hat{\boldsymbol{x}}$ contains the estimates of unknowns, obtained by applying the weighted least-squares method to (8). These estimates might not be precisely equal to their corresponding true values because of measurement errors incurred in practice.

C. Identifying the Faulted Line and Fault Type

The system of equations (8) is derived assuming that the line *i-j* is the faulted line. The Weighted Sum of Squared Residuals (*WSSR*) is the objective function minimized for solving (8) by the least-squares method and can be obtained from.

$$WSSR = [\boldsymbol{m} - \boldsymbol{H}\hat{\boldsymbol{x}}]^* \boldsymbol{R}^{-1} [\boldsymbol{m} - \boldsymbol{H}\hat{\boldsymbol{x}}] \tag{11}$$

The *WSSR* of the faulted line would be ideally zero as all measurements hold true in equations (5) to (7). However, due to measurement/parameter imperfections, the *WSSR* of the faulted line might not be exactly zero but very small [18]. Accordingly, (11) should be evaluated for different suspected lines to identify the smallest *WSSR*, thus the faulted line. Once $\hat{\boldsymbol{x}}$ is estimated, the superimposed voltages at any buses, including the faulted line terminals, can be obtained by (5). Having calculated the superimposed voltage and current phasors at the faulted line terminals, the closed-form expression introduced in [31] can be used to obtain the fault distance on the faulted line. The calculated fault distance is checked to ensure it lies within the acceptable range to enhance the security of the proposed scheme.

Full network observability is not required by the proposed scheme, in which the entire KVL and KCL equations related to voltage and current measurement are utilized for deriving an overdetermined system of linear equations with reference to the short-circuit fault. In principle, each system of equations can be uniquely solved when there are a sufficient number of independent equations in the respective system. This condition can readily be verified offline for any PMU placement given [18].

4. Modify the superimposed circuit for WABP

As explained, every PEIRES circuit can be modeled as an unknown current source in each superimposed sequence. As suggested by [18], this current can be directly measured by a PMU. However, it may not be practical to install a PMU at every bus with a PEIRES. Even if there is a PMU at all PEIRES buses, WABP must not be contingent on the availability of a specific set of PMU measurements. As discussed in IEEE standard C37.118.2, communication latency is unavoidably unpredictable and may vary from a few milliseconds to even seconds due to factors such as error checking, forwarding, and routing. Therefore, some PMU measurements might not be received within the action time necessary for successful WABP. On the other hand, having a large number of non-measured unknown currents representing PEIRESs in the vector $\hat{\boldsymbol{x}}$ might lead to an unsolvable system of equations, thus, no *WSSRs* to act upon [18,32].

It is fair to assume that the control strategies of PEIRESs and their corresponding settings are available to the control center. The knowledge of these may be used to overcome the foregoing unsolvability challenge. The goal is to reduce the number of unknowns to the extent that (8) becomes solvable with a unique solution. To this end, a sufficient number of the PEIRESs in the negative-sequence circuit can be replaced by their equivalent superimposed impedances. In doing so, the operating modes of PEIRESs are first determined using the superimposed technique and SCADA data. Next, the equivalent superimposed impedances of the selected PEIRESs are calculated and incorporated into the superimposed circuit. Since PEIRESs exhibit different equivalent impedance after reaching their overcurrent limits, their estimated output currents are to be checked, as well. Appropriate modifications will then be applied in order to update their equivalent superimposed impedances.

A. PEIRES Operating Mode Following a Fault

Following a short-circuit fault, PEIRESs may work in either steady-state or fault mode. In the steady-state mode, they inject active and reactive power equal to pre-set references. In the fault mode, the operating references are adjusted based on the Grid Code requirements to support the grid in fault conditions. The amount of positive-sequence voltage dip at a PEIRES terminal determines the PEIRES's operating mode. For instance, if the balanced voltage dip is larger than 10%, the PEIRES should operate in the fault mode (as instructed by the GB and Tennet Grid Codes). As detailed in [28], the equivalent positive-sequence impedance of a PEIRES in the superimposed circuit depends on the pre-fault voltage and current phasors. Hence, PEIRESs with no PMUs at their terminals cannot be easily modeled in the superimposed positive-sequence circuit.

To determine PEIRESs' operating modes, the following steps are taken in this paper to estimate positive-sequence voltage dips whilst maintaining the computational burden low:

  i. PEIRESs whose currents are not directly measured by PMUs are firstly disregarded in the superimposed circuit. This is to approximately estimate positive-sequence superimposed voltages using the described superimposed circuit technique.
 ii. Approximate post-fault bus voltages are calculated in this step. Based on the Superposition Theorem, post-fault bus voltages can be obtained from the pre-fault and superimposed bus voltages, i.e. $V_{post}^p = V_{pre}^p + \Delta V^p$. Superimposed bus voltages are approximated in step (i). Pre-fault bus voltages are assumed to be known in the control center. This can be easily achieved by effective state estimation methods employing existing synchronized/ unsynchronized measurements [33].
iii. Ignoring PEIRES contributions to the fault current introduces some errors in the estimated post-fault voltage quantities. The contributions of PEIRESs operating in the fault mode are more significant to the inaccuracy introduced than that of PEIRESs operating in the steady-state mode. This is because PEIRESs operating in steady-state mode continue to inject the same active and reactive power even after the fault inception. Accordingly, the PEIRESs are arranged in descending order with respect to voltage dips at their terminals. The PEIRESs on top of the list can be replaced by unknown current sources and included in the vector x to increase accuracy. This will be applied to as many PEIRESs as possible as long as the matrix $\boldsymbol{H}$ remains of full rank, which is a sufficient condition for the solvability of (8) [32]. This helps to obtain more accurate approximations for post-fault bus voltages.
 iv. Let us assume that for voltage dips larger than α%, the PEIRES is set to operate in the fault mode by injecting extra reactive power. The value of α is dictated by the Grid Code requirements. The

estimated post-fault voltages in step (iii) might not be quite accurate because some PEIRESs have not been replaced by a current source.

v. All PEIRESs experiencing voltage dips close to α are considered to have an uncertain operating mode. Special care should be taken to determine the upper and lower bounds of the uncertain voltage range. As demonstrated in [34], however, the impact of control strategies of a PEIRES connected to the grid barely exceeds 5% of its terminal voltage. This means that we are almost certain that PEIRESs with estimated voltage dips less than $(\alpha - 5)$% will continue to operate in the steady-state mode. On the other hand, those with estimated voltage dips greater than $(\alpha + 5)$% can be assumed to be operating in the fault mode. Next, an additional step is needed to confirm the operating mode of PEIRESs with estimated voltage dips between the thresholds mentioned above.

The fault behavior of the PEIRES (from the power system point of view) is dependent on the converter control strategies and settings and feasible bounds rather than the type of energy source [24]. Various types of renewables might demonstrate slightly different transient behavior for a few milliseconds following the fault inception. Regardless of the type of renewable sources, however, they will be able to regulate the amplitude and phase angle of their terminal voltage and current to meet their control targets in the steady-state, fault, and post-fault conditions within a few milliseconds [24]. Therefore, the proposed formulation is not impacted by the type of renewable sources. On the other hand, the proposed scheme is expected to come into effect in case the primary protection has failed to operate. Thus, a few hundred milliseconds is available for WABP to account for the time that PEIRESs need to completely switch to their final operating modes before making a trip decision [1,2].

B. Incorporating PEIRESs Models

If a PEIRES operates in the steady-state mode, it does not generate a post-fault negative-sequence current. Due to the absence of the pre-fault negative-sequence components, the superimposed negative-sequence current of that PEIRES will be zero and can be removed from (9). Accordingly, the corresponding column in the matrix H is removed. The negative-sequence behavior of a PEIRES operating in the fault mode depends on its control strategy. If there is no information about the control strategies of a PEIRES at the control center, it will be modeled as an unknown nodal current source in the WABP formulations (8). Otherwise, it is incorporated in the superimposed circuit based on its control strategy, as described below.

1) Suppressing negative-sequence current

As described in Subsection II-A, a PEIRES with this control strategy eliminates the negative-sequence current during an asymmetrical fault. Similar to the PEIRES operating in the steady-state mode, the PEIRES can be omitted from the circuit, i.e., modeled by an open circuit.

2) Eliminating the active or reactive power ripple

A PEIRES operating in the fault mode can be modeled as an impedance in the superimposed circuit. As detailed in [28], the magnitude and phase angle of the per-unit equivalent negative-sequence impedance of a PEIRES, i.e. $|z^n|$ and θ^n, with these control strategies can be calculated as follows:

$$|z^n| = \frac{1}{\sqrt{\left(\frac{P_{ref}}{(V^p)^2 - K(V^n)^2}\right)^2 + \left(\frac{Q_{ref}}{(V^p)^2 + K(V^n)^2}\right)^2}} \qquad (12)$$

$$\theta^n = \tan^{-1}\left(\frac{Q_{ref}}{P_{ref}} \cdot \frac{(V^p)^2 - K(V^n)^2}{(V^p)^2 + K(V^n)^2}\right) - (K+1) \times 90^o \qquad (13)$$

where V^n and V^p are the positive- and negative-sequence terminal voltages of the PEIRES. The inclusion of the equivalent impedances of PEIRESs with this control strategy is not straightforward because their equivalent impedance is not always known a priori. As (12) and (13) demonstrate, the equivalent negative-sequence impedance of a PEIRES is determined by its control strategy, active and reactive power reference values, and the voltage dip it undergoes due to the fault. That is why we need to resort to an iterative method here. An approximate value for V^p can be calculated as described in part A of this section. It is assumed that the control strategy and reference values are received from SCADA. According to (12) and (13), z^n is represented as a function of ΔV^n, i.e. $f_1(\Delta V^n)$. Based on (5), the value of ΔV^n is affected by z^n itself. Thus, it is represented as a function of z^n, i.e. $f_2(z^n)$. Herein, a numerical iterative method is utilized to estimate the values of z^n and ΔV^n as follows:

(i). The PEIRES is firstly removed from the superimposed circuit. Then, the initial value of ΔV^n is estimated using the described superimposed circuit technique.

(ii). The amount of z^n is calculated using (12) and (13).

(iii). The PEIRES is replaced with impedance z^n in the superimposed circuit. Then, the value of ΔV^n is updated.

(iv). The previous two steps are repeated until the new value of z^n lies within 1% proximity of its previous value.

3) Imitating an impedance in the negative-sequence circuit

The PEIRES operating in this mode represents a constant impedance, say $z^n = |z^n| \angle \theta^n$, in the negative-sequence circuit during an asymmetrical fault. Due to the absence of pre-fault negative-sequence components, the post-fault negative-sequence circuit is equivalent to its superimposed circuit. Therefore, the PEIRES can be substituted by the pre-set impedance z^n in the superimposed circuit.

C. Considering Overcurrent Limits of PEIRESs

Once a PEIRES reaches its overcurrent limit in the negative-sequence circuit, the reference currents calculated in (2) and (4) will no longer be valid. This results in an equivalent impedance differing from what it was before reaching the overcurrent limit. Therefore, it is necessary to check if the overcurrent limit of a PEIRES is reached during a fault. If this is the case, proper modification to the obtained equivalent impedance will be applied.

Reference-current saturation is the most common current-limiting logic [28], which is also considered for limiting the negative-sequence current of PEIRESs in this paper. In doing so, if the total negative-sequence current exceeds a threshold, i.e. i_{max}^n, the corresponding reference currents are tunned as.

$$\begin{cases} i_{d-ref}^{n,new} = \frac{i_{max}^n}{\sqrt{\left(i_{d-ref}^n\right)^2 + \left(i_{q-ref}^n\right)^2}} \times i_{d-ref}^n \\[4mm] i_{q-ref}^{n,new} = \frac{i_{max}^n}{\sqrt{\left(i_{d-ref}^n\right)^2 + \left(i_{q-ref}^n\right)^2}} \times i_{q-ref}^n \end{cases} \qquad (14)$$

As a result, if a PEIRES reaches its negative-sequence current limit, the magnitude of its equivalent negative-sequence impedance can be obtained as follows.

$$|z^n|_{min} = \frac{|\Delta V^n|}{i_{max}^n} \qquad (15)$$

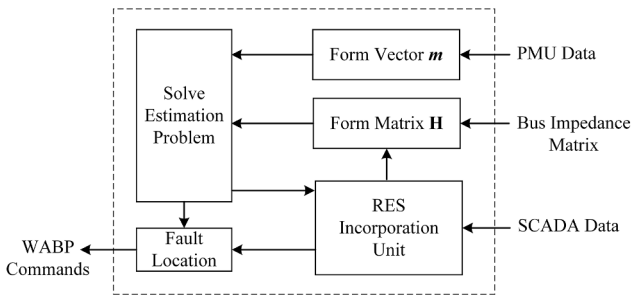The values of ΔV^n is itself a function of z^n as in (5). Thus, an
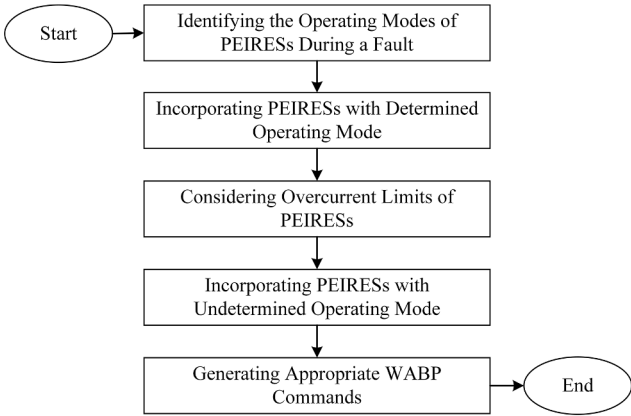
Fig. 3. Conceptual diagram of the proposed WABP scheme.

Fig. 4. Flowchart of the functions of the "*PEIRES Incorporation Unit*".

Table 1
Control Strategies/Settings and Locations of PEIRESs.

Location (Bus No.)	Control Strategy	Control Setting
1,17	Suppressing Negative Sequence Current	$i_{max}^n = 0$, Sn = 100 MVA, $P_{ref} = 0.8$ pu, $Q_{ref} = 0.2$ pu
2,6,9,13,14,18,22	Mitigating Active Power Ripple	$i_{max}^n = 0.3$, Sn = 150 MVA, $P_{ref} = 0.9$ pu, $Q_{ref} = 0.1$ pu
3,7,10,15,19,28	Mitigating Reactive Power Ripple	$i_{max}^n = 0.4$, Sn = 150 MVA, $P_{ref} = 0.9$ pu, $Q_{ref} = 0.1$ pu
4,5,8,12,20,21,24	Imitating an Impedance	$i_{max}^n = 0.4$, Sn = 150 MVA, $P_{ref} = 0.9$ pu, $Q_{ref} = 0.1$ pu, $z^n = 0.3 \angle 90^o$

transmission systems. The "*PEIRES Incorporation Unit*" module is in charge of dealing with uncertainties in the bus-impedance matrix due to the operating status of PEIRESs and regulating *H* matrix based on their different control strategies. A flowchart of the functions of the "*PEIRES Incorporation Unit*" is shown in Fig. 4, which has already been detailed in parts *A* to *D*. Once the operating modes of all PEIRESs in the power system are determined, the *WSSR* is updated for the candidate line. Finally, the transmission line corresponding to the minimum *WSSR* is identified as the faulted line. To enhance the security of the proposed scheme, the calculated fault distance on the pinpointed line is checked to ensure it is real and lies within the acceptable range [0,1].

5. Performance evaluation

The performance of the proposed WABP scheme is evaluated by conducting more than 80,000 simulations on the IEEE 39-bus test system with different penetration levels of PEIRESs. For each set of PEIRESs added to the system, their total active power is proportionally deducted from the active power produced by the existing synchronous generators so that the total active power generation (around 6200 MW) is maintained constant. A general performance evaluation for different asymmetrical fault types at various locations with an arbitrary set of PEIRESs is presented first. Next, the sensitivity of the proposed scheme to measurement errors, line/generator parameters errors, and pre-fault negative-sequence components is examined. The impact of different numbers and locations of PMUs is also scrutinized. Finally, the performance of the proposed scheme is tested for various penetration levels and locations of PEIRESs with different control strategies and settings. For the PEIRES control loops, a second-order generalized integrator [34] is used to apply *i* representing a 90° phase shift in the time domain in (1).

DIgSILENT PowerFactory is used to carry out the simulations. Time-domain voltage and current waveforms are first filtered by an anti-aliasing Butterworth filter with a cut-off frequency of 400 Hz. The current measurements for generation transformers are taken from their high-voltage sides, e.g., the delta winding side of the step-up transformer of PEIRESs. Accordingly, the angle displacements caused by the transformers are incorporated in equations (5) to (7). Time-domain measurements are then sampled with a frequency of 2 kHz. The discrete Fourier transform (DFT) is used to estimate the phasors of the recorded time-domain waveforms. Any other effective phasor estimation methods, such as the real PMU model in [35], could be used to provide more accuracy if needed.

A. General Evaluation of the Proposed Scheme

An arbitrary set of 22 PEIRESs with different control strategies and settings are added to the 39-bus system, as detailed in Table 1. This set of PEIRESs is also applied for parts *B, C, D,* and *E* in this section. Buses 3, 5, 8, 11, 14, 16, 19, 23, 25, 27, 29 and 39 are equipped with PMUs [36], which are also valid for parts B, C, D, and F. The model and other parameters of simulated PEIRESs are listed in the Appendix.

As explained, the proposed scheme estimates the voltage dips at PEIRESs to determine their operating modes and the way they are

algorithm is needed to incorporate the overcurrent limit of PEIRESs operating in the fault mode. The detailed procedure used in this paper is as follows.

(i) The amplitude of the negative-sequence current of the PEIRES is calculated via $I_{PEIRES}^n = |\Delta V^n|/|z^n|$. If I_{PEIRES}^n exceeds i_{max}^n, the magnitude of the z^n representing the PEIRES is replaced by $|z^n|_{min}$.
(ii) The new value of ΔV^n is estimated.
(iii) Equation (15) is employed to update $|z^n|_{min}$.
(iv) The previous two steps are repeated until the new value of $|z^n|_{min}$ lies within 1% proximity of its previous value.

D. Checking PEIRESs with <u>Uncertain</u> Mode

From PEIRESs experiencing voltage dips within the uncertain range ($\alpha \pm$ 5)%, those with voltage dips closer to α% at their terminals are replaced by nodal current sources. This means they are incorporated into the vector *x* as extra unknown variables and are removed from the bus impedance matrix. This will be applied to as many PEIRESs as possible to the extent that the matrix *H* still remains of full rank. Next, the remaining PEIRESs with uncertain operating modes are scrutinized to determine their true operating modes.

As explained in [18], the more accurate the *H* matrix, the smaller the minimum *WSSR* obtained. Therefore, the targeted PEIRES is temporarily assumed to be operating in the opposite (fault or steady-state) mode. Accordingly, the required amendments are applied to the *H* matrix. Then, the new value of minimum *WSSR* is calculated. If the minimum *WSSR* is reduced, it follows that the PEIRES under consideration is truly operating in the opposite mode. Otherwise, it is operating in the predefined mode found in Subsection IV-A.

E. Flowchart of the proposed scheme

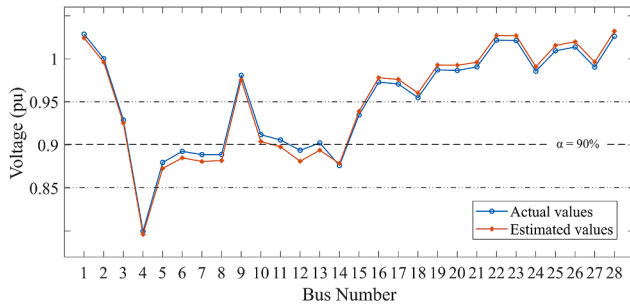Fig. 3 shows a conceptual diagram of the proposed WABP scheme for

Fig. 5. Actual and initial estimation of post-fault voltage profile at PEIRES locations.

incorporated, i.e., by a current source or an equivalent impedance. To demonstrate the capability of the proposed scheme for doing so, a solid 1-ph-g fault at 95% of line 3–4 is explored. As per the GB Grid Code, PEIRESs undergoing voltage dips of more than 10% are set to operate in the fault mode. Fig. 5 shows the initial estimation of the post-fault voltage profile and the actual voltage profile at 80 ms following the fault inception. Accordingly, Table 2 reports the identified operating modes of PEIRESs and the way that each one is incorporated in the WABP formulation. As can be seen from Fig. 5, the estimated voltage dips of some PEIRESs are within the uncertain range. However, the operating modes of all PEIRESs are finally identified correctly. The amplitude and angle errors between the real and the estimated negative-sequence current or impedance of PEIRESs are combined into a single error quantity referred to as total vector error (TVE) [37], and listed in the last column of Table 2. Fig. 6 depicts the WSSRs of all lines for up to 300 ms after the fault inception. As can be seen, the smallest WSSR correctly indicates the true faulted line with sufficient distinction from other candidate lines. The fault location result for this case has only 0.19% error from its actual value.

Due to indefinite wide-area communication latencies, the proposed scheme cannot be employed for primary protection but for backup protection. As mentioned, a few hundred milliseconds is available for WABP before making a trip decision [1,2]. Nonetheless, WABP should be fast enough and be able to make a reliable decision once enough PMU data are received at the control center. A limited number of multiplication and addition operations is needed to calculate the required PEIRES equivalent impedances and the scalar index WSSR for each candidate line. According to extensive simulations conducted, less than three iterations are required for every iterative step on average. The average computation time of the whole procedure is about 50 ms, on a 2.8 GHz processor with 8 GB of RAM, which is less of a concern than communication latencies in the context of decision time available for WABP. It should be noted that for bigger power systems, the proposed WABP can be efficiently limited to the disturbed area whose boundaries are observed by PMUs. This approach has already been presented and successfully tested in [18]. Besides, the related process can also be effectively parallelized on both software and hardware levels. Further progress in communication technology to reduce the communication latencies can allow the implementation of the proposed scheme for the main protection in the future.

Table 3 summarizes the main characteristics of the most effective WABP schemes in the literature that are insensitive to fault resistance and independent of local protective relays. As can be seen, the proposed

scheme can account for the presence of PEIRESs while outperforming other schemes in many aspects, such as tolerance against PMU losses, low computational burden, and independence of specific PMU placement. According to Table 3, since the scheme presented in [18] has better characteristics than other schemes listed, the performance of the proposed scheme is only compared with that of [18].

The proposed method does not operate following symmetrical faults as no significant negative sequence quantity will be present under such conditions. To show the effectiveness of the proposed WABP scheme, various types of asymmetrical faults are applied at different locations on every line in the system with fault resistances of 0 Ω, 20 Ω, and 100 Ω. In each case, the calculated fault location is averaged over 80–300 ms following the fault inception. The performance of the proposed scheme is compared to that of the WABP scheme presented in [18]. Simulations show that the presence of PEIRESs has a more significant influence on the success rate of faulted-line identification for faults closer to substations. Thus, only results for faults on the first and last 20% of line lengths are reported. Table 4 summarizes obtained results in terms of Faulted-Line Identification Success Rate (FLISR) and Average Fault Location Error (AFLE). As explained, the operating modes of the PEIRES are automatically identified by the scheme. Accordingly, another index reported in Table 4 is PEIRES Operating Mode Identification Success Rate (POMISR). It can be seen that the proposed scheme successfully pinpoints the faulted line irrespective of the fault resistance with a success rate of more than 99% on average. As expected, the scheme presented in [18] demonstrates a noticeably lower accuracy and success rate for not considering the presence of PEIRESs. This clearly demonstrates the superiority of the proposed scheme over the existing scheme in the presence of PEIRESs, given the reliability requirements for protection applications [1–2].
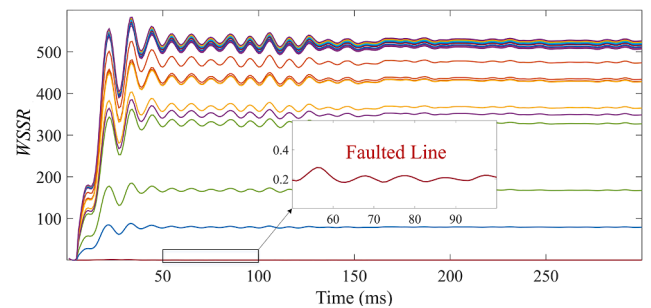
Fig. 6. *WSSRs* of different candidate lines calculated over time following a solid 1-ph-g fault at 95% of line 3–4.

Table 3
Comparison between the Main Characteristics of Different WABP Schemes.

Comparison aspect	[13,15]	[14,17]	[16]	[18]	Prop.
Tolerate PMU losses?	No	Yes	Yes	Yes	Yes
Need specific PMU placement?	Yes	No	No	No	No
Computation burden	Low	Low	High	Low	Low
Need statuses of local relays?	No	No	No	No	No
Sensitivity to fault resistance	Low	Low	Low	Low	Low
Address the presence of PEIRESs?	No	No	No	No	Yes

Table 2
Performance of the Proposed WABP Scheme for a Solid 1-ph-g Fault at 95% of Line 3–4.

Detected Operating Mode	Incorporation Method	PEIRES Bus No.	Ave. TVE	Max. TVE
Steady-State Mode	N/A	1,2,3,9,10,15,17,18,19,20,21,22,24,28	N/A	N/A
Fault Mode	Replace by a current source	5,8,13,14	1.82%	2.74%
	Replace by an impedance	4,6,7,12	4.08%	7.75%

Table 4
General Performance of the Proposed WABP Scheme.

Fault Type	Results	Proposed Scheme			Scheme in [18]		
		0 Ω	20 Ω	100 Ω	0 Ω	20 Ω	100 Ω
Single Phase to Ground	FLISR (%)	99.64	99.78	100	85.22	91.25	95.3
	AFLE (%)	0.56	0.61	0.74	6.89	4.23	2.74
	POMISR (%)	99.63	99.83	99.86	N/A	N/A	N/A
Phase to Phase	FLISR (%)	100	100	100	87.43	90.85	94.92
	AFLE (%)	0.44	0.48	0.56	6.58	4.63	3.04
	POMISR (%)	99.08	99.45	99.58	N/A	N/A	N/A
Two Phase to Ground	FLISR (%)	98.53	99.07	99.32	85.96	90.56	94.81
	AFLE (%)	0.54	0.61	0.69	7.11	5.84	3.21
	POMISR (%)	99.08	99.57	99.66	N/A	N/A	N/A

B. Sensitivity to Measurement Errors

To simplify the compliance specification of PMUs, amplitude and angle error bounds are combined into TVE quantities. Here, TVE is a measure of the difference between the phasor reported by the PMU and the true phasor. The performance of the proposed scheme with input phasors having different ranges of TVEs is studied in this Subsection. To this end, 100 arbitrary asymmetrical faults are applied at different locations throughout the transmission system. The fault resistance is set to have a random value between 0 Ω and 50 Ω. Measurement errors are assumed to have a normal distribution around the true value of corresponding phasors. Each simulated case is repeated 100 times for reporting FLISR and AFLE. The obtained results are tabulated in Table 5, where the three-sigma criterion is used for reporting the error range [18]. As expected, larger measurement errors result in less success rate for the proposed scheme. From a practical point of view, the proposed scheme proves to have sufficient robustness against measurement errors as it functions correctly for more than 98.81% of the cases with up to 5% measurement errors.

C. Sensitivity to Parameter Errors

In this Subsection, the impact of transmission line and generator parameter errors on the success rate of the proposed WABP scheme is

Table 5
WABP Sensitivity to Measurement Errors.

Results	Variation Range for Measurement Errors (%)				
	±1	±2	±3	±4	±5
FLISR (%)	99.42	99.36	99.21	99.14	98.81
AFLE (%)	0.57	0.60	0.64	0.72	0.83

Table 6
WABP Sensitivity to Line Parameter Errors.

Results	Variation Range of Line Parameter Errors (%)				
	±1	±2	±3	±4	±5
FLISR (%)	99.21	98.82	98.35	97.77	97.33
AFLE (%)	0.72	1.15	1.76	2.32	3.07

Table 7
WABP Sensitivity to Generator Parameter Errors.

Results	Variation Range of Generator Parameter Errors (%)				
	±1	±2	±3	±4	±5
FLISR (%)	99.42	99.34	99.13	98.92	98.73
AFLE (%)	0.54	0.62	0.78	0.96	1.09

scrutinized. Tables 6 and 7 summarize obtained results when lines and generators are considered to have random parameter errors within different ranges. The same short-circuit faults as those in the previous Subsection are examined in this study. Each simulated case is repeated 100 times for reporting FLISR and AFLE. As expected, the success rate of the scheme decreases as the variation range of parameter errors increases. Practically speaking, the success rate still remains in an acceptable range, even for errors of up to 5%.

D. Sensitivity to Pre-Fault Negative Sequence Components

Grid Codes dictate the maximum negative sequence voltage caused by voltage unbalance to be maintained below certain small values [38]. For instance, the maximum permissible voltage unbalance allowed by the GB Grid Code is 1.5% in the transmission grid. This requirement is to be strictly followed by system operators to avoid the damaging impact of the negative sequence components on rotating machines. To scrutinize the impact of the pre-fault negative sequence components, up to 1.5% negative-sequence voltages are induced at different buses in the pre-fault condition by making load and line parameters slightly unbalanced. The success rate of the proposed algorithm in this condition with fault resistances of 0 Ω, 20 Ω, and 100 Ω is reported in Table 8. As can be seen, permissible pre-fault negative sequence components do not noticeably impair the performance of the proposed scheme.

E. Observability and PMU Coverage

Full network observability is not a prerequisite for the proposed scheme to function properly. However, the variance of the estimated unknowns in (10) can be obtained by $\left(\boldsymbol{H}^{*}\boldsymbol{R}^{-1}\boldsymbol{H}\right)^{-1}$ [39], which means a greater number of PMUs provides higher accuracy.

Further simulations show that installing a PMU in poorly PMU-

Table 8
WABP Sensitivity to Pre-Fault Negative Sequence Components.

Results	Up to 1.5% Pre-Fault Voltage Unbalance			No Pre-Fault Voltage Unbalance		
	0 Ω	20 Ω	100 Ω	0 Ω	20 Ω	100 Ω
FLISR (%)	99.06	98.83	99.74	99.39	99.62	99.77
AFLE (%)	0.73	0.84	0.91	0.51	0.57	0.67

Table 9
WABP Sensitivity to the Number of PMUs.

Results	Number of PMUs				
	12	11	10	9	8
FLISR (%)	98.92	98.02	97.60	96.84	96.01
AFLE (%)	1.10	1.26	1.47	1.76	1.82

Table 10
WABP Sensitivity to Control Strategy/Settings, Number, and Locations of PEIRES.

Scenario No.	Results	Number of PEIRES				
		28	24	20	16	12
1 *	FLISR (%)	99.46	99.50	99.68	99.68	99.72
	AFLE (%)	0.66	0.64	0.52	0.50	0.50
	POMISR (%)	99.51	99.56	99.69	99.68	99.71
2 *	FLISR (%)	99.36	99.40	99.46	99.56	99.56
	AFLE (%)	0.63	0.61	0.59	0.59	0.58
	POMISR (%)	99.62	99.31	99.39	99.42	99.42
3 *	FLISR (%)	99.38	99.46	99.48	99.54	99.54
	AFLE (%)	0.56	0.55	0.55	0.53	0.52
	POMISR (%)	99.54	99.33	99.36	99.43	99.45
4 *	FLISR (%)	99.32	99.36	99.38	99.42	99.50
	AFLE (%)	0.67	0.62	0.58	0.57	0.55
	POMISR (%)	99.77	99.76	99.78	99.79	99.78
5 **	FLISR (%)	99.34	99.36	99.44	99.47	99.50
	AFLE (%)	0.62	0.60	0.59	0.58	0.56
	POMISR (%)	99.71	99.71	99.73	99.74	99.76

* All PEIRESs are set to 1) suppress neg. seq. current, 2) mitigate active power ripple, 3) mitigate reactive power ripple, 4) imitate an impedance.
** Every PEIRES is randomly set to one of the foregoing control strategies.

covered areas increases the success rate of faulted line identification. To demonstrate this, the performance of the proposed scheme is studied with different numbers of PMUs. For each specific number of PMUs, 50 randomly created placements leading to a solvable system of equations with a unique solution have been considered. The FLISR and AFLE indices obtained for the foregoing set of asymmetrical faults are summarized in Table 9. As can be seen, larger numbers of PMUs result in more accurate and reliable results. It can be concluded that the more intensely PMUs cover the fault area, the bigger the *WSSRs* of other candidate locations. This also shows that missing data of a few PMUs would not adversely affect the scheme's performance.

F. Impact of PEIRES Locations and Control Strategies

This Subsection studies the impact of the number, location, and control strategies/settings of PEIRESs on the scheme's performance. The total active power generated in the system is maintained constant to obtain different penetration levels of PEIRESs. For each specific number of PEIRESs, 50 randomly created placements have been considered. To examine the impact of PEIRES control strategies, five different scenarios are defined for each PEIRES placement. For the first to fourth scenarios, one of the control strategies described in Section II is selected and applied to all PEIRESs. In the fifth scenario, the control strategy of each PEIRES is randomly selected. The control settings of each PEIRES, i.e., S_n, P_{ref}, Q_{ref}, i_{max}^n, $|z^n|$, and θ^n are randomly selected within [100, 150] MVA, [0.85, 0.95] pu, [0.1, 0.3] pu, [0.2, 0.4] pu, [0.2, 0.6] pu, and [60°, 90°], respectively.

The FLISR and AFLE indices obtained for a set of 100 asymmetrical short-circuit faults are summarized in Table 10. In the proposed scheme, all PEIRESs are accurately modeled by an impedance or replaced by a current source. As a result, the number, location, and control strategies/settings of PEIRESs do not have a noticeable adverse effect on the performance of the scheme.

6. Conclusion

This paper puts forward a wide-area backup protection (WABP) scheme for transmission systems with high penetration of renewable energy sources. An efficient technique is proposed to capture the behavior of non-synchronous generations during faults based on their control strategies. The formulations are focused on four well-established negative-sequence control strategies of power electronics interfaced

renewable energy sources (PEIRESs) in the literature. The superimposed circuit technique is used for deriving an overdetermined system of linear equations with reference to the short-circuit fault in question. This results in robust fault location based upon the weighted sum of squared residuals (*WSSR*) concept.

It is also demonstrated that modeling all PEIRESs as unknown current sources may render the system of equations unsolvable. As detailed in the paper, this can be avoided by modeling a limited number of PEIRESs as current sources. The rest should be modeled by an equivalent impedance according to their control strategies/settings and overcurrent limits. Replacing PEIRESs by equivalent impedances involves more computational burden but will give rise to the same accurate results, as verified by extensive simulations. The extra computational burden can be seen as the price paid for not imposing any rigid constraints on PMU numbers and locations. A total of more than 80,000 simulations conducted show that the proposed scheme is highly robust against factors such as measurement and parameter errors. The proposed scheme outperforms existing WABP schemes in a wide variety of conditions examined. This is the case irrespective of the asymmetrical fault type, PEIRES penetration level, locations, and control strategies. As the proposed scheme does not require full network observability, missing data of a few PMUs would not noticeably affect its performance. Thanks to the foregoing advantages, the authors believe that the proposed scheme is a step forward in the context of promoting and encouraging practical implementations of WABP.

CRediT authorship contribution statement

Mohammad Rezaei Jegarluei: Conceptualization, Methodology, Software, Writing – original draft. **Petros Aristidou:** Resources, Investigation, Validation. **Sadegh Azizi:** Writing – review & editing, Formal analysis, Validation, Supervision.

Declaration of Competing Interest

The authors declare that they have no known competing financial interests or personal relationships that could have appeared to influence the work reported in this paper.

Data availability

No data was used for the research described in the article.

Appendix: Model and Parameters of PEIRESs

PEIRESs are modeled as static generators in DIgSILENT PowerFactory. The parameters of simulated PEIRESs and the applied controllers, other than those in Table 1, are listed in Table A1.

Table A1
Model and Parameters of PEIRESs.

Plant Category	Renewable Generation
Technology	Three phase
Number of Parallel Units	30
Proportional Gain of PLL	10
Integration Gain of PLL	30
Prop. Gain of Curr. Controller (d- and q-axis)	1
T. Cons. of Curr. Controller (d- and q-axis)	4 ms
Impedance of the Series Reactor	0.1 pu
Positive Sequence Control Strategy	Based on the GB Grid Code
Positive Sequence Maximum Curr.	1 pu

References

[1] Phadke AG, Thorp JS. *Computer relaying for power systems*. Wiley Online. Library 2009.

[2] Horowitz SH, Phadke AG. Power system relaying. 4th ed. John Wiley & Sons; 2008.

[3] Telukunta V, Pradhan J, Agrawal A, Singh M, Srivani SG. Protection challenges under bulk penetration of renewable energy resources in power systems: a review. CSEE J Power Energy Syst Dec. 2017;3(4):365–79.

[4] Jones KW, Pourbeik P, Kobet G. Impact of inverter-based generation on bulk power system dynamics and short-circuit performance. NERC Task Force Short-Circuit Syst. Perform. Impact Inverter Based Gener., Atlanta, GA, USA, Rep. PESTR68, 2018.

[5] Brahma SM, Girgis AA. Development of adaptive protection scheme for distribution systems with high penetration of distributed generation. IEEE Trans Power Del Jan. 2004;19(1):56–63.

[6] Haddadi A, Zhao M, Kocar I, Karaagac U, Chan KW, Farantatos E. Impact of inverter-based resources on negative sequence quantities-based protection elements. IEEE Trans on Power Del Feb. 2021;36(1):289–98.

[7] Nagpal M, Henville C. Impact of power-electronic sources on transmission line ground fault protection. IEEE Trans Power Del Feb. 2018;33(1):62–70.

[8] Wu Y-K, Lin Z-T, Lee T-C, Hsieh T-Y, Lin W-M. Adaptive setting and simulation of distance protection relay in a long transmission system connected to and offshore wind farm. J Clean Energy Technol 2016;4(6):401–7.

[9] Hooshyar A, Azzouz MA, El-Saadany EF. Distance protection of lines emanating from full-scale converter-interfaced renewable energy power plants – Part II: solution description and evaluation. IEEE Trans Power Del Aug. 2015;30(4): 1781–91.

[10] Barati J, Seifossadat SG, Joorabian M. A new adaptive coordination scheme of distance relays in DFIG - based wind farm collector lines and transmission line compensated by STATCOM. Int Trans Electr Energy Syst 2021;31(12):Dec.

[11] Xie X, Zhan Y, Liu H, Li W, Wu C. Wide-area monitoring and early-warning of subsynchronous oscillation in power systems with high penetration of renewables. Int J Elect Power Energy Syst Jun. 2019;108:31–9.

[12] Terzija V, et al. Wide-area monitoring, protection, and control of future electric power networks. Proc IEEE Jan. 2011;99(1):80–93.

[13] Mirhosseini S, Akhbari M. Wide-area backup protection algorithm for transmission lines based on fault component complex power. Int J Elect Power Energy Syst Dec. 2016;83:1–6.

[14] Majidi M, Etezadi-Amoli M, Fadali MS. A sparse-data-driven approach for fault location in transmission networks. IEEE Trans Smart Grid Mar. 2017;8(2):548–56.

[15] Neyestanaki MK, Ranjbar AM. An adaptive PMU-based wide area backup protection scheme for power transmission lines. IEEE Trans Smart Grid May 2015;6 (3):1550–9.

[16] Dobakhshari AS. Wide-area fault location of transmission lines by hybrid synchronized/unsynchronized voltage measurements. IEEE Trans Smart Grid May 2018;9(3):1869–77.

[17] Azizi S, Sanaye-Pasand M. A straightforward method for wide-area fault location on transmission networks. IEEE Trans Power Del Feb. 2015;30(1):441–5.

[18] Azizi S, Sanaye-Pasand M. From available synchrophasor data to short-circuit fault identity: formulation and feasibility analysis. *IEEE Trans Power Syst* May 2017;32 (3):2062–71.

[19] Azizi S, Liu G, Dobakhshari AS, Terzija V. Wide-area backup protection against asymmetrical faults using available phasor measurements. IEEE Trans Power Del Dec 2019.

[20] Chavez JJ, et al. PMU-voltage drop based fault locator for transmission backup protection. Electr Power Syst Res 2021;196.

[21] Jegarluei MR, Dobakhshari AS, Azizi S. Reducing the computational complexity of wide-area backup protection in power systems. IEEE Trans Power Del Jun. 2022;37 (3):2421–4.

[22] Jegarluei MR, Cortés JS, Azizi S, Terzija V. Wide-area event identification in power systems: A review of the State-of-the-Art. IEEE International Conference on Smart Grid Synchronized Measurements and Analytics May 2022:1–7.

[23] Shalini, Samantaray SR. A differential voltage-based wide-area backup protection scheme for transmission network. IEEE Systems Journal Feb 2021.

[24] Chaudhuri N, Chaudhuri B, Majumder R, Yazdani A. Multi-terminal direct-current grids: modeling, analysis, and control. John Wiley & Sons; 2014.

[25] Khan MAU, Hong Q, Egea-Àlvarez A, Dyśko A, Booth C. A communication-free active unit protection scheme for inverter dominated islanded microgrids. International Journal of Electrical Power & Energy Systems Nov. 2022;142: p108125.

[26] Biswal S, Swain SD, Patidar RD, Bhoi AK, Malik OP. Integrated wide-area backup protection algorithm during stressed power system condition in presence of wind farm. Arabian J Sci Eng Jan. 2021;8:1–14.

[27] Song X, Wang Y, Hu W, Wang Z. Three reference frame control scheme of 4 wire grid-connected inverter for microgrid under unbalanced grid voltage conditions. Proc. IEEE APECE Feb. 2009:1301–5.

[28] Jia K, Yang Z, Fang Y, Bi T, Sumner M. Influence of inverter interfaced renewable energy generators on directional relay and an improved scheme. IEEE Trans Power Electron Dec. 2019;34(12):11843–55.

[29] Aji H, Ndreko M, Popov M, van der Meijden MAMM. Investigation on different negative sequence current control options for MMC-HVDC during single line to ground AC faults. In: 2016 IEEE PES Innovative Smart Grid Technologies Conference Europe (ISGT-Europe); 2016. p. 1–6.

[30] Technische Regeln für den Anschluss von Kundenanlagen an das Hochspannungsnetz und deren Betrieb (TAR Hochspannung), VDEARN 4120 Anwendungsregel: 2018-11.

[31] Johns AT, Jamali S. Accurate fault location technique for power transmission lines. IEE Proc. C, Gener., Transm., Distrib. Nov. 1990;137(6):395–402.

[32] Meyer CD. Matrix analysis and applied linear algebra. Philadelphia, PA, USA: SIAM; 2001.

[33] Dobakhshari AS, Azizi S, Paolone M, Terzija V. Ultra-fast linear state estimation utilizing SCADA measurements. IEEE Trans Power Syst Jul. 2019;34(4):2622–31.

[34] Kabiri R, Holmes DG, McGrath BP. Control of active and reactive power ripple to mitigate unbalanced grid voltages. IEEE Trans. Ind. Appl. Mar. 2016;52(2):1660–8.

[35] Romano P, Paolone M. Enhanced interpolated-DFT for synchrophasor estimation in FPGAs: theory, implementation, and validation of a PMU prototype. IEEE Trans Instrum Meas Dec. 2014;63(12):2824–36.

[36] Azizi S, Dobakhshari AS, Sarmadi SAN, Ranjbar AM. Optimal PMU placement by an equivalent linear formulation for exhaustive search. IEEE Trans Smart Grid Mar. 2012;3(1):174–82.

[37] IEEE Standard for Synchrophasor Measurements for Power Systems, IEEE Std. C37.118.1-2011, 2011.

[38] Ghassemi F, Perry M. Review of voltage unbalance limit in the GB Grid Code CC.6.1.5 (b). Accessed: Jul. 11, 2020. [Online]. Available: https://www.nationalgrid.com.

[39] Schweppe FC, Wildes J. Power system static-state estimation, Part I: Exact model. IEEE Trans on Power Apparatus and system 1970;89(1):Jan.